

This is an Open Access document downloaded from ORCA, Cardiff University's institutional repository: <https://orca.cardiff.ac.uk/id/eprint/98381/>

This is the author's version of a work that was submitted to / accepted for publication.

Citation for final published version:

Korbar, Tvrtko, McDonald, Iain , Premec Fucek, Vlasta, Fucek, Ladislav and Posilovic, Hrvoje 2017. Post-impact event bed (tsunamite) at the Cretaceous-Palaeogene boundary deposited on a distal carbonate platform interior. *Terra Nova* 29 (2) , pp. 135-143. 10.1111/ter.12257

Publishers page: <http://dx.doi.org/10.1111/ter.12257>

Please note:

Changes made as a result of publishing processes such as copy-editing, formatting and page numbers may not be reflected in this version. For the definitive version of this publication, please refer to the published source. You are advised to consult the publisher's version if you wish to cite this paper.

This version is being made available in accordance with publisher policies. See <http://orca.cf.ac.uk/policies.html> for usage policies. Copyright and moral rights for publications made available in ORCA are retained by the copyright holders.



Terra Nova

Post-impact event bed (tsunamite) at the Cretaceous– Paleogene boundary deposited on a distal carbonate platform interior

Journal:	<i>Terra Nova</i>
Manuscript ID	TER-2016-0078.R2
Wiley - Manuscript type:	Paper
Date Submitted by the Author:	n/a
Complete List of Authors:	Korbar, Tvrtko; Croatian Geological Survey, Department of Geology MacDonald, Iain; School of Earth, Ocean and Planetary Sciences, Cardiff University Premec Fuček, Vlasta; INA-Industrija nafte d.d., Exploration Sector Fuček, Ladislav; Croatian Geological Survey, Department of Geology Posilović, Hrvoje; Croatian Geological Survey, Department of Geology
Keywords:	Cretaceous-Paleogene boundary, asteroid impact, carbonate platform, event bed, tsunamite

1 Running head: K–Pg boundary event bed on carbonate platform

2

3 Post-impact event bed (tsunamite) at the Cretaceous–Paleogene

4 boundary deposited on a distal carbonate platform interior

5 Tvrтко Korbar¹, Iain McDonald², Vlasta Premec Fuček³, Ladislav Fuček¹, Hrvoje Posilović¹

6

7 ¹ Croatian Geological Survey, Department of Geology, Sachsova 2, HR-10000 Zagreb, Croatia.

8 ² School of Earth, Ocean and Planetary Sciences, Cardiff University, Park Place, Cardiff CF10 3AT, United

9 Kindom.

10 ³ INA-Industrija nafte d.d., Exploration Sector, Lovinčićeva 4, HR-10000 Zagreb, Croatia.

11

12 **ABSTRACT**

13 **We show crucial evidence for the Cretaceous–Paleogene (K–Pg) boundary event recorded**
14 **within a rare succession deposited in an inner-platform lagoon on top of a Mesozoic,**
15 **tropical, intra-oceanic (western Tethys) Adriatic carbonate platform, that is exposed at**
16 **Likva cove on the island of Brač (Croatia). The last terminal Maastrichtian fossils appear**
17 **within a distinct 10–12 cm thick event bed that is characterized by soft-sediment**
18 **bioturbation and rare shocked-quartz grains, and is interpreted as a distal tsunamite.**
19 **Directly overlying this is 2 cm thick reddish-brown clayey mudstone containing planktonic**
20 **foraminifera typical for the basal Danian, and with elevated platinum-group elements in**
21 **chondritic proportions indicating a clear link to the Chicxulub asteroid impact. These**
22 **results strongly support the first discovery of the “potential” K–Pg boundary tsunamite on**
23 **the neighboring island of Hvar, and these two complementary sections represent probably**
24 **the most complete record of the event among known distal shallow-marine successions.**

25

26

27 Introduction

28 The Chicxulub asteroid impact (Alvarez *et al.*, 1980; Smit and Hertogen, 1980; Schulte *et al.*, 2010)
29 triggered global mass extinctions and extraordinary sedimentary perturbations at the Cretaceous–Paleogene
30 (K–Pg) boundary some 66 million years ago (Renne *et al.*, 2013). Within distal sedimentary successions
31 around the globe, the boundary is marked by a thin clay horizon containing elevated concentrations of
32 platinum-group elements (PGE), along with shocked mineral grains and spherules from the impact fallout
33 (e.g., Bohor and Izett, 1986; Alvarez *et al.*, 1990; Smit, 1999; Montanari and Koeberl, 2000; Glass and
34 Simonson, 2013). While deep-water successions have been extensively studied (Smit 1999; Klaus *et al.*,
35 2000; Claeys *et al.*, 2002; MacLeod *et al.*, 2007; Esmeray-Senlet *et al.*, 2015), including ichnofossils and
36 discontinuities at the boundary (e.g., Rodríguez-Tovar and Uchman, 2008; Alegret *et al.*, 2015),
37 comparatively less is known about shallow-water perturbations in distal regions (Steuber and Schlüter,
38 2012). Although carbonate platform successions in the peri-Adriatic region (Fig. 1) commonly exhibit a
39 hiatus that includes the K–Pg transition (Eberli *et al.*, 1993; Bosellini *et al.*, 1999; Vlahović *et al.* 2005;
40 Korbar 2009), the boundary interval has recently been documented on the island of Hvar in Croatia (Korbar
41 *et al.*, 2015). The K–Pg boundary is tentatively indicated also within the Likva section on the neighboring
42 island of Brač, but only negative evidence for the boundary has previously been reported for this site
43 (Jelaska and Ogorelec, 1983; Gušić and Jelaska, 1990; Steuber *et al.*, 2005). In this paper, we present a
44 focused sedimentological, biostratigraphic, and geochemical study of the central part of the Likva section,
45 including an exceptional occurrence of the impact ejecta and the K–Pg boundary “clay” containing isolated
46 specimens of index planktonic foraminifera that are very rare within carbonate platform successions. Thus,
47 the Likva section on Brač provides additional details missing in the “potential” K–Pg boundary tsunamite
48 firstly discovered on the neighboring island of Hvar (Korbar *et al.*, 2015),

49

50 Geological setting

51 The present-day peri-Adriatic area (central-northern Mediterranean) represents the deformed
52 sedimentary cover of the Adriatic microplate or Adria – the Mesozoic northern promontory of Africa

53 (Channell *et al.*, 1979). The Mesozoic Adriatic carbonate platform (ACP) was a low-latitude, mainly
54 shallow-marine system comparable to the modern Bahama banks (Eberli *et al.*, 1993; Vlahović *et al.*, 2005),
55 situated in the central part of Adria within central-western Tethys (Fig. 1). Cenozoic deformation of the
56 Mesozoic platform carbonates was controlled by Alpine orogenesis, forming a complex fold-and-thrust belt
57 of the External Dinarides along the northeast margin of the Adriatic Sea (Korbar 2009).

58

59 **Material and methods**

60 The island of Brač is built predominantly of ACP carbonates (Fig. S1) and the K–Pg succession is
61 exposed at Likva cove (43.389° N, 16.460° E; Figs. S1 and S2). The succession is a few tens of meters thick
62 and characterized by typical shallow-water carbonates of the Sumartin Formation, indicating inner-platform,
63 peritidal depositional environments (Jelaska and Ogorelec, 1983; Gušić and Jelaska, 1990; Steuber *et al.*,
64 2005).

65 The suspected K–Pg interval was logged, macroscopically analyzed in the field, and sampled (Fig.
66 2). Standard polished slabs and thin sections were used for petrographic and micropaleontological
67 assessments, following Flügel (2010). Planktonic foraminifera were successfully isolated only from a softer
68 sample of the K–Pg “clay” on the smallest sieve (45 µm), and photographed by scanning electron
69 microscopy (SEM) at INA (Zagreb). Taxonomic classification of Paleocene planktonic foraminifera
70 identified in this study follows the work of Olsson *et al.* (1999), and Koutsoukos (2014), as well as the
71 planktonic foraminiferal biozonation of Wade *et al.* (2011).

72 Nine limestone samples (5–10 g in mass) were analyzed for PGE and gold at Cardiff University (UK)
73 using nickel sulfide fire assay followed by Te co-precipitation and inductively coupled plasma mass
74 spectrometry (ICP-MS) as described in McDonald and Viljoen (2006). Data are given in supplementary
75 Table S1. Selected limestone samples were dissolved in 10% HCl. The quartz grains were etched with 10%
76 HF for five to ten minutes, and were analyzed and photographed on SEM coupled with energy dispersive
77 spectrometer at CGS (Zagreb).

78

79 **Results**

80 The uppermost Maastrichtian miliolid limestones at Likva (facies “2.6.” of Jelaska and Ogorelec,
81 1983), the type level of *Fleuryana adriatica* (De Castro *et al.*, 1994), are characterized in the topmost part
82 by a 70 cm thick succession of skeletal-peloidal limestone lithotypes (the uppermost bed of the interval “C”
83 of Steuber *et al.*, 2005). The succession comprises 4 intervals (numbers 1-4 on Fig. 2A), separated by flat or
84 undulating discontinuities. From the base upwards: 20 cm thick requieniid rudist floatstone of interval 1; 8-
85 15 cm thick packstone of interval 2; 25-32 cm thick wackestone of interval 3; and 10-12 cm thick packstone-
86 grainstone of interval 4. Interval 4 (Figs. 2B-D, S2B-C, S3) is a distinct single depositional unit that is
87 directly overlain by 2 cm of reddish-brown clayey mudstone – equated with the K–Pg boundary “clay” (Fig.
88 2B).

89 Intervals 1-4 contain a diversified Maastrichtian benthic association, while rare planktonic
90 foraminifera and pithonellid calcispheres are only found in the wackestones of interval 3 (Fig. 3A). Besides
91 various miliolids, benthic foraminifera recognized in these limestones are: *Fleuryana adriatica*, *Laffitteina*
92 *mengaudi*, *Bolivinopsis* sp., Discorbidae, Rotaliidae, Ophthalmidiidae, and Valvulinidae, along with
93 Ostracoda, *Thaumatoporella parvovesiculifera*, and Charophyta (calcareous brackish algae). Sr isotope
94 stratigraphy data of Steuber *et al.* (2005) confirm the terminal Maastrichtian age of interval 1 that contains
95 the last appearance of requieniid rudists *Apricardia* sp., as well as the last appearance of rudists in life-
96 position within the ACP succession. Interval 3 is indistinctly bioturbated, while the topmost few cm are
97 characterized by irregular dark grey traces of intergranular infiltrations from above (Fig. 2A).

98 Interval 4 has an undulating lower boundary (Fig. S1C) and a discontinuous bioclastic lag composed
99 of requieniid rudist bioclasts (up to 10 mm long, Figs. 2C, 3B), as well as dark grey intraclasts of
100 wackestone that is similar to interval 3 (Fig. 2C). The fossil assemblage is the same as in the intervals below,
101 with the addition of unusual calcitic spherules characterized by rough exterior and complex sparitic-micritic
102 walls (40-60 µm in diameter, Figs. 2D, 3C). The spherules are sparsely distributed throughout the interval 4,
103 along with very rare detrital quartz grains (up to 60 µm in diameter). Interval 4 is marked by distinct
104 reddish-brown, tubular (2-3 mm in diameter) bioturbation (Figs. 2B, C, S3) filled by finer-grained peloidal-
105 bioclastic wackestones containing microbioclasts and Maastrichtian benthic foraminifera (Fig. 2D). The
106 color is dispersed around tiny darker reddish-brown micritic carbonate grains with iron oxides and traces of

107 iron phosphates that are irregularly distributed within the bioturbation. The HCl insoluble residuum of whole
108 interval 4 rock contains dark grey organic matter, rare shocked quartz grains (30-100 μm in diameter
109 displaying multiple sets of closely spaced planar deformation features (PDFs), some 40 grains per 1 dm^3 of
110 limestone, Fig. 4), potassium feldspars, pyroxene (diopside), kaolinite and (mainly framboidal) pyrite.

111 The clayey mudstone directly overlying interval 4 contains ostracods (Fig. 3D) and rare tiny
112 planktonic foraminifera typical for the indistinct basal Danian Zones P0-P α (Fig. 5). PGE are highly
113 enriched in the mudstone, with respect to the other limestones (Fig. 2A, Table S1). High temperature PGE
114 (Os, Ir, Ru, and Rh) in both the clayey mudstone and interval 4 are nearly chondritic but [Pt/Ir]N, [Pd/Ir]N
115 and [Au/Ir]N are suprachondritic (Table S1) reflecting a crustal PGE component (Koeberl *et al.* 2012).
116 Hydrogen sulfide release during treatment with HCl indicated dissolution of sulfides (probably pyrite). The
117 insoluble residuum consists of kaolinite and illite.

118 The overlying 6-8 cm thick mudstone (interval 5) is characterized by thalassinoid bioturbation, and
119 contains ostracods, tiny planktonic foraminifera (tentatively P α -P1a zones according to thin-section
120 determination of *Subbotina* cf. *trivialis*, *Globanomalina* cf. *planocompressa*, and *Eoglobigerina* cf.
121 *eobulloides*), and rare small benthic foraminifera (*Bangiana hanseni*, *Rotorbinella hermi*, *Laffitteina* sp., and
122 tiny miliolids). The overlying >60 cm thick mudstone-wackestones of the intervals 6-8 are characterized by
123 rare planktonic foraminifera and a gradual increase in diversity and proportion of benthic foraminifera,
124 microgastropods, and Characean algae.

125

126 Discussion

127 This study shows that the uppermost Maastrichtian miliolid limestones in Likva cove on the island of
128 Brač are characterized by polyspecific (predominantly benthic) communities, indicating a subtidal inner-
129 platform environment that differs from the underlying intertidal laminites (Jelaska and Ogorelec, 1983). The
130 presence of some brackish taxa (Characean algae) suggests at least occasional influence of fresh water, while
131 rare planktonic foraminifera (Fig. 3A) and pithonellid calcispheres in interval 3 also indicate an influence
132 from the open sea within what is interpreted as a semi-enclosed lagoon on top of a tide-dominated ACP
133 interior. This association is unusual but in accordance with the most recent data on eustatic sea-level rise

134 during the latest Maastrichtian (Esmeray-Senlet *et al.*, 2015), related to the increased SST that is recorded
135 even at high latitudes (Witts *et al.*, 2016).

136 Considering the depositional setting, its distinctive appearance, erosional lower boundary, rip-up
137 clasts, and bioclastic lag, interval 4 could be interpreted as an event bed – possibly a distal carbonate
138 platform tsunamite rather than storm deposit (Morton *et al.*, 2007), because even major storms are known to
139 have little impact on modern tide-dominated platform-top sedimentation (Boss *et al.*, 1993; Rankey *et al.*,
140 2004). Thus, probably only a major tsunami surge, that can be considered as an extraordinary tide, is capable
141 to make such a distinct event bed within the platform interior on modern and ancient carbonate platforms
142 (see discussion in Korbar *et al.*, 2015).

143 The complex calcitic spherules from interval 4 (Figs. 2D and 3C) do not resemble simple Late
144 Cretaceous marine pithonellid calcispheres found in interval 3, that are common also in open carbonate
145 platform facies of the ACP (e.g., Korbar *et al.*, 2012). Interestingly, the spherules more closely resemble
146 Paleozoic calcispheres (cf. Plate 66/1-3 of Flügel, 2010) and Proterozoic impact spherules (cf. Fig. 7.8 of
147 Glass and Simonson, 2013). Although the original composition of impact spherules can be changed during
148 diagenesis (Montanari *et al.*, 1983; Montanari, 1991), spherules from the event bed are probably of biogenic
149 origin, possibly fresh-water or hypersaline calcispheres displaced from a pond by the tsunami.

150 The slightly elevated Os, Ir and Ru concentrations in interval 4 are chondritic (Table S1), and given
151 the association with shocked quartz, support the idea of sparsely re-distributed and diagenetically altered
152 ejecta within the tsunamite. Similar PGE values are detected on top of the Majerovica K–Pg tsunamite on
153 the island of Hvar (Korbar *et al.*, 2015) and likely represent the same depositional event. Majerovica is
154 currently situated 24 km south of Likva cove (Fig. S1), and probably >40 km 66 myr ago. Furthermore,
155 precise biostratigraphy of the directly overlying K–Pg “clay” with its chondritic PGE (Fig. 2A, Table S1),
156 strongly supports direct correlation between the two sites and with the K–Pg trans-Atlantic tsunami triggered
157 by the Chicxulub impact (Norris *et al.*, 2000; MacLeod *et al.*, 2007; Korbar *et al.*, 2015).

158 The truly global significance of the K–Pg boundary in the Likva section, however, comes from the
159 sedimentary structures and the microfossils that are preserved. Smooth edges and morphology of the
160 bioturbation in interval 4 suggest soft-sediment burrowing by annelid worms – polychaetes (Herringshaw *et*

161 *al.*, 2010), while finer-grained infill and non-carbonate minerals suggest changes of physical and
162 geochemical characters of the pristine deposit. According to studies on modern analogues, polychaetes are
163 the most abundant benthic non-skeletal macrofauna in tropical, shallow-water, intraoceanic carbonate
164 sediments, especially in lagoons (e.g., Frouin and Hutchings, 2001). Most polychaetes are non-selective
165 surface deposit feeders that ingest marine sediment, and the processing time for the sediment can be as little
166 as 15 minutes (Rouse and Pleijel, 2001). However, some annelids are selective deposit feeders that seek
167 particles of a specific size, and their processing time may cover 2-2.5 hours (Bock and Miller, 1999).
168 Importantly, decay of sediment particles processed by the deposit-feeding organisms is faster because of
169 digestion (Needham *et al.*, 2004).

170 The Chicxulub impact ejecta layer is fairly uniform in thickness (2-3 mm) at distances of 7000–
171 11000 km (Smit, 1999). Ballistic and most of relatively coarser-grained non-ballistically distributed impact
172 ejecta probably reached the most globally distal sites within several hours (Artemieva and Morgan, 2009),
173 while the post-impact landslide tsunami likely took 10-20 hours to reach the ACP (Fig. 1; Norris *et al.*,
174 2000; Ward, 2001; Korbar *et al.*, 2015). The expected delay between arrival of ballistic ejecta and the
175 tsunami was probably long enough for the deposit-feeding polychaetes to ingest some of the deposited ejecta
176 particles of the optimal size (Bock and Miller, 1999). Following the surge of the very distal and attenuated
177 tsunami over the ACP top, and deposition of 10-12 cm thick tsunamite in the lagoon, passively transported
178 and temporarily buried animals would attempt to escape from the relatively thick sand blanket. Intensive
179 burrowing by polychaetes during the hours to days after the deposition (Herringshaw *et al.*, 2010) is a
180 probable cause of a lack of an expected thin mudcap from the uppermost part of the deposit. Ingested
181 ballistic ejecta could be reworked along with later non-ballistic, early deposited impact dust from the top of
182 the tsunamite into the burrows to produce Os, Ir, and Ru, enrichment in interval 4. The clay minerals could
183 originate from ejecta, degraded firstly during digestion (Needham *et al.*, 2004), and subsequently during
184 diagenesis (Montanari, 1991).

185 The K–Pg “clay” (Fig. 2B), i.e., lime mud mixed with settling impact dust and aerosols, was
186 deposited in the lagoon during the sudden decrease in carbonate production, which lasted decades to
187 millennia, as a result of a global “impact-winter” (Galeotti *et al.*, 2004; Vellekoop *et al.*, 2014).

188 Nevertheless, that 2-cm thick horizon had to be deposited during the time needed for evolution of new
189 species of planktonic foraminifera (Fig. 5) defining the first Danian Zones P0 and P α , i.e. during at least the
190 first ten millennia of the Cenozoic (Koutsoukos, 2014). Increasing abundance and variability of benthic
191 fossils in mudstones of the interval 5, tentatively assigned to the zones P α -P1a, suggest that shallow-water
192 carbonate factory recovered during the next few tens of thousands years (Wade *et al.*, 2011).

193

194 **Conclusions**

195 The tsunamite at Likva represents probably the most distal reported sedimentary record of the K–Pg
196 boundary tsunami that is much thinner but more complete than at Majerovica (Korbar *et al.*, 2015). These
197 two sections together strongly support the hypothesis about the K–Pg boundary tsunami on the ACP.

198 Environmental effects in the marine realm in the immediate aftermath of the Chicxulub impact are
199 incompletely recorded in many of the well-known distal deep-water K–Pg boundary sections around the
200 world (Claeys *et al.*, 2002; Schulte *et al.*, 2010), because of a slow settling of the ejecta through the water
201 column (Stokes's Law), discontinuities in the sedimentary record (Alegret *et al.*, 2015), and the absence of
202 the tsunami reworking (Smit, 1999). In contrast, shallow-water successions can preserve evidence for the
203 first hours following impact, especially shallow-marine (sub)tropical carbonates because of early
204 cementation. However, shallow-water deposits are also more prone to subsequent reworking or erosion, and
205 the exceptional preservation found at Likva offers an important new opportunity for further research into the
206 both immediate aftermath one of the most catastrophic global events in Earth's history, and a recovery of a
207 carbonate factory at the beginning of Cenozoic.

208

209 **Acknowledgements**

210 We thank to Renata Slavković for SEM images of planktonic foraminifera, Katica Drobne for
211 determination of some Paleocene benthic foraminifera, and Alessandro Montanari for a previous fruitful
212 discussion on the topic and some suggestions for the methodology. We thank also to the Editors as well as to
213 Bruce M. Simonson, Francisco J. Rodríguez-Tovar, R. Mark Leckie, and an anonymous reviewer for their
214 constructive reviews.

215

216 **References**

217 Alegret, L., Rodríguez-Tovar, F.J., and Uchman, A., 2015. How bioturbation obscured the Cretaceous–Paleogene
218 boundary record. *Terra Nova*, **27**, 225-230.

219 Alvarez, L.W., Alvarez, W., Asaro, F., and Michel, H.V., 1980. Extraterrestrial cause for the Cretaceous-Tertiary
220 extinction. *Science*, **208**, 1095-1108.

221 Alvarez, W., Asaro, F., and Montanari, A., 1990. Ir profile for 10 Myr across the Cretaceous-Tertiary boundary at
222 Gubbio (Italy). *Science*, **250**, 1700-1702.

223 Artemieva N., and Morgan J., 2009. Modeling the formation of the K Pg boundary layer. *Icarus*, **201**, 768-780.

224 Bock, M.J. and Miller, D.C., 1999. Particle selectivity, gut volume, and the response to a step change in diet for
225 deposit feeding polychaetes. *Limnol. Oceanogr.*, **44**, 1132-1138.

226 Bohor, B.F., and Izett, G., 1986. Worldwide size distribution of shocked quartz at the K/T boundary: Evidence for a
227 North American impact site. *Lunar Planet. Sci.*, **17**, 68-69.

228 Bosellini, A., Morsilli, M., and Neri, C., 1999. Long-term event stratigraphy of the Apulia platform margin (Upper
229 Jurassic to Eocene, Gargano, southern Italy). *J. Sed. Res.*, **69**, 1241-1252.

230 Boss, S.K., and Neumann, A.C., 1993. Impacts of Hurricane Andrew on carbonate platform environments, north Great
231 Bahama Bank. *Geology*, **21**, 897-900.

232 Channell, J.E.T., D'Argenio, B., and Horvath, F., 1979. Adria, the African promontory, in Mesozoic Mediterranean
233 palaeogeography. *Earth-Sci. Rev.*, **15**, 213-292.

234 Claeys, P.H., Kiessling, W., and Alvarez, W., 2002. Distribution of Chicxulub ejecta at the Cretaceous-Tertiary
235 boundary. In: *Catastrophic Events and Mass Extinctions: Impacts and Beyond* (C.,Koeberl and K.G. MacLeod,
236 eds). *Geol. Soc. America Spec. Paper*, **356**, 55-68.

237 De Castro, P., Drobne, K., and Gušić, I., 1994. *Fleuryana adriatica* n. gen., n. sp. (Foraminiferida) from the uppermost
238 Maastrichthian of the Brač island (Croatia) and some other localities on the Adriatic carbonate platform.
239 *Rasprave IV. razreda SAZU* (Ljubljana), **35**, 129-149.

240 Eberli, G.P., Bernoulli, D., Sanders, D., and Vecsei, A., 1993. From aggradation to progradation: the Maiella platform
241 (Abruzzi, Italy). In: *Cretaceous carbonate platforms* (A.J. Simo, R.W. Scott, and J.-P. Masse, eds). *Mem.*
242 *American Assoc. Petrol. Geol.*, **56**, 213-232.

- 243 Esmeray-Senlet, S., Özkan-Altiner, S., Altiner, D., and Miller, K.G., 2015. Planktonic foraminiferal biostratigraphy,
244 microfacies analysis, sequence stratigraphy, and sea-level changes across the Cretaceous–Paleogene boundary
245 in the Haymana basin, central Anatolia, Turkey. *J. Sed. Res.*, **85**, 489-508.
- 246 Flügel, E., 2010. *Microfacies of Carbonate Rocks*: Heidelberg, Springer, 984 pp.
- 247 Frouin, P., and Hutchings, P., 2001. Macrobenthic communities in a tropical lagoon (Tahiti, French polynesia, central
248 Pacific). *Coral Res.*, **19**, 277-285.
- 249 Galeotti, S., Brinkhuis, H., and Huber, M., 2004. Records of postCretaceous-Tertiary boundary millennial-scale
250 cooling from the western Tethys: A smoking gun for the impact-winter hypothesis? *Geology*, **32**, 529-532.
- 251 Glass, B.P., and Simonson, B.M., 2013. Distal Impact Ejecta Layers. In: *Impact Studies* (C. Koeberl, ed). Heidelberg,
252 Springer, 716 pp.
- 253 Gušić, I., and Jelaska, V., 1990. Stratigrafija gornjokrednih naslaga otoka Brača u okviru geodinamske evolucije
254 Jadranske karbonatne platforme (Upper Cretaceous stratigraphy of the Island of Brač within the geodynamic
255 evolution of the Adriatic carbonate platform). *Djela Jugoslavenske akademije znanosti i umjetnosti* (Zagreb),
256 **69**, 160 pp.
- 257 Herringshaw, L.G., Sherwood, O.A., and McIlroy, D., 2010. Ecosystem engineering by bioturbating polychaetes in
258 event bed microcosms. *Palaios*, **25**, 46-58.
- 259 Jelaska, V., and Ogorelec, B., 1983. The Upper Cretaceous depositional environments of the carbonate platform on the
260 Island of Brač (Stop 10). In: *Contribution to Sedimentology of Some Carbonate and Clastic Units of Coastal*
261 *Dinarides* (LJ. Babić, and V. Jelaska, eds). 4th I.A.S. regional meeting, Split, Excursion Guide-book, 99-124.
- 262 Klaus, A., Norris, R.D., Kroon, D., and Smit, J., 2000. Impact-induced K-T boundary mass wasting across the Blake
263 Nose, W. North Atlantic. *Geology*, **28**, 319-322.
- 264 Koeberl, C., Claeys, P., Hecht, L., and McDonald, I., 2012. Geochemistry of impacts. *Elements*, **8**, 37-42.
- 265 Korbar, T., 2009. Orogenic evolution of the External Dinarides in the NE Adriatic region: A model constrained by
266 tectonostratigraphy of Upper Cretaceous to Paleogene carbonates. *Earth-Sci. Rev.*, **96**, 296-312.
- 267 Korbar, T., Glumac, B., Cvetko Tešovic, B., and Cadieux, S.B., 2012. Response of a carbonate platform to the
268 Cenomanian-Turonian drowning and OAE2: A case study from the Adriatic Platform (Dalmatia, Croatia). *J.*
269 *Sed. Res.*, **82**, 163-176.

- 270 Korbar, T., Montanari, A., Premec Fuček, V., Fuček, L., Coccioni, R., McDonald, I., Claeys, P., Schulz, T., and Koeberl,
271 C., 2015. Potential Cretaceous-Paleogene boundary tsunami deposit in the intra-Tethyan Adriatic Carbonate
272 Platform section of Hvar (Dalmatia, Croatia). *Geol. Soc. America Bull.*, **127**, 1666-1680.
- 273 Koutsoukos, E.A.M., 2014. Phenotypic plasticity, speciation, and phylogeny in early Danian planktic foraminifera. *J.*
274 *Foram. Res.*, **44**, 109-142.
- 275 MacLeod, K.G., Whitney, D.L., Huber, B.T., and Koeberl, C., 2007. Impact and extinction in remarkably complete
276 Cretaceous-Tertiary boundary sections from Demerara Rise, tropical western North Atlantic. *Geol. Soc.*
277 *America Bull.*, **119**, 101-115.
- 278 McDonald, I., and Viljoen, K.S., 2006. Platinum-group element geochemistry of mantle eclogites: a reconnaissance
279 study of xenoliths from the Orapa kimberlite, Botswana. *Appl. Earth Sci. (Trans. Inst. Min. Metall. B)*, **115**,
280 B81-93.
- 281 Montanari, A., 1991. Authigenesis of impact spheroids in the K/T boundary clay from Italy: new constraints for high-
282 resolution stratigraphy of terminal Cretaceous events. *J. Sediment. Petrol.*, **61**, 315-339.
- 283 Montanari A., and Koeberl, C., 2000. Impact stratigraphy: The Italian record: Heidelberg, Springer, 364 Pp.
- 284 Montanari A., Hay R.L., Alvarez W., Asaro F., Michel H.V., Alvarez L.W., and Smit J., 1983. Spheroids at the
285 Cretaceous-Tertiary boundary are altered impact droplets of basaltic composition. *Geology*, **11**, 668-671.
- 286 Morton, R.A., Gelfenbaum, G., and Jaffe, B.E., 2007. Physical criteria for distinguishing sandy tsunami and storm
287 deposits using modern examples: *Sed. Geol.*, **200**, 184-207.
- 288 Needham, S.J., Worden, R.H., and McIlroy, D., 2004. Animal-sediment interactions: The effect of ingestion and
289 excretion by worms on mineralogy. *Biogeosciences*, **1**, 113-121.
- 290 Norris, R.D., Firth, J., Blusztajn, J., and Ravizza, G., 2000. Mass failure of the North Atlantic margin triggered by the
291 Cretaceous/Paleogene bolide impact. *Geology*, **28**, 1119-1122.
- 292 Olsson, R.K., Hemleben, C., Berggren, W.A., and Huber, B.T., 1999. Atlas of Paleocene planktonic foraminifera.
293 Smithsonian Contributions to Paleobiology, **85**, 252 pP.
- 294 Rankey, E.C., Enos, P., Steffen, K., and Druke, D., 2004. Lack of impact of Hurricane Michelle on tidal flats, Andros
295 Island, Bahamas: Integrated remote sensing and field observations. *J. Sed. Res.*, **74**, 654-661.
- 296 Renne, P.R., Deino, A.L., Hilgen, F.J., Kuiper, K.F., Mark, D.F., Mitchell III, W.S., Morgan, L.E., Mundil, R., and
297 Smit, J., 2013. Time scales of critical events around the Cretaceous-Paleogene Boundary. *Science*, **339**, 684-
298 687.

- 299 Rodríguez-Tovar, F.J., and Uchman, A., 2008. Bioturbational disturbance of the Cretaceous–Palaeogene (K–Pg)
300 boundary layer: Implications for the interpretation of the K–Pg boundary impact event: *Geobios*, **41**, 661–667.
- 301 Rouse, G.W., and Pleijel, F., 2001. Polychaetes. Oxford University Press, 349 pp.
- 302 Smit, J., 1999, The global stratigraphy of the Cretaceous-Tertiary boundary impact ejecta: *Ann. Rev. Earth and Planet.*
303 *Sci.*, **27**, 75-113.
- 304 Smit, J., and Hertogen, J., 1980. An extraterrestrial event at the Cretaceous-Tertiary boundary. *Nature*, **28**, 198-200.
- 305 Schulte, P., Alegret, L., Arenillas, I., Arz, J.A., Barton, P.J., Brown, P.R., Bralower, T.J., Christeson, G.L., Claeys, P.,
306 Cockell, C.S., Collins, G.S., Deutsch, A., Goldin, T.J., Goto, K., Grajales-Nishimura, J.M., Grieve, R.A.F.,
307 Gulick, S.P.S., Johnson, K.R., Kiessling, W., Koeberl, C., Kring, D.A., Macleod, K.G., Matsui, T., Melosh, J.,
308 Montanari, A., Morgan, J.V., Neal, C.R., Nichols, D.J., Norris, R.D., Pierazo, E., Ravizza, G., Rebolledo-
309 Vieyra, M., Reimond, W.U., Robin, E., Salge, T., Speijer, R.P., Sweet, A.R., Urrutia-Fucugauchi, J., Vajda, V.,
310 Whalen, M.T., and Willumsen, P.S., 2010. The Chicxulub asteroid impact and mass extinction at the
311 Cretaceous-Paleogene Boundary. *Science*, **327**, 1214-1218.
- 312 Scotese, C.R., and Dreher, C., 2012. Global Geology. <http://www.globalgeology.com/>
- 313 Steuber, T., and Schlüter, M., 2012. Strontium-isotope stratigraphy of Upper Cretaceous rudist bivalves: Biozones,
314 evolutionary patterns and sea-level change calibrated to numerical ages. *Earth-Sci. Rev.*, **114**, 42-60.
- 315 Steuber, T., Korbar, T., Jelaska, V., and Gušić, I., 2005. Strontium-isotope stratigraphy of Upper Cretaceous platform
316 carbonates of the Island of Brač (Adriatic Sea, Croatia): Implications for global correlation of platform
317 evolution and biostratigraphy. *Cretac. Res.*, **26**, 741-756.
- 318 Vellekoop, J., Sluijs, A., Smit, J., Schouten, S., Weijers, J.W.H., Sinninghe Damsté, J.S., and Brinkhuis, H., 2014.
319 Rapid short-term cooling following the Chicxulub impact at the Cretaceous–Paleogene boundary. *Proc. Nat. Ac.*
320 *Sci.* **111**, 7537-7541.
- 321 Vlahović, I., Tišljarić, J., Velić, I., and Matičec, D., 2005. Evolution of the Adriatic Carbonate Platform:
322 Palaeogeography, main events and depositional dynamics. *Palaeogeogr. Palaeoclimatol. Palaeoecol.*, **220**, 333-
323 360.
- 324 Wade, B.S., Pearson, P.N., Berggren, W.A., and Palike, H., 2011. Review and revision of Cenozoic tropical
325 planktonic foraminiferal biostratigraphy and calibration to the geomagnetic polarity and astronomical time
326 scale. *Earth-Sci. Rev.*, **104**, 111-142.
- 327 Ward, S.N., 2001. Landslide Tsunami. *J. Geoph. Res.*, **106**, 11201-11215.

328 Witts, J.D., Whittle, R.J., Wignall, P.B., Crame, J.A., Francis, J.E, Newton, R.J., and Bowman, V.C., 2016.
329 Macrofossil evidence for a rapid and severe Cretaceous–Paleogene mass extinction in Antarctica. *Nat.*
330 *Commun.* 7:11738, doi: 10.1038/ncomms11738

331 .

332

333 **FIGURE CAPTIONS**

334

335 **Fig. 1** Simplified Cretaceous–Paleogene (K–Pg) paleogeography showing Chicxulub impact site (red
336 circles), hypothetical traces of east propagated intercontinental tsunami (white broken lines), and Likva
337 locality (red arrow) on the Adriatic Carbonate Platform (modified from [Korbar *et al.*, 2015](#) according to
338 [Scotese and Dreher, 2012](#)). Brown – land, light blue – neritic, dark blue – bathyal and abyssal.

339

340 **Fig. 2** (A) Outcrop photograph and simple stratigraphic column of the Cretaceous–Paleogene (K–Pg)
341 boundary succession within a middle part of Sumartin Formation at Likva cove, showing intervals and
342 obtained concentrations of PGEs and gold (numbers in small frames on the photograph mark exact position
343 of the PGE samples, [Table S1](#)). (B) The reddish-brown K–Pg boundary clayey mudstone (“clay”) contains
344 planktonic foraminifera typical for basal Danian P0–P α zones (see [Fig. 5](#)). The underlying event bed
345 (Interval 4) contains the last appearance of Maastrichtian fossils, and is characterized by small intraclasts
346 (arrow) ripped-up from the directly underlying wackestone of the interval 3, and rudist bioclasts in the lower
347 part, along with distinct reddish-brown soft-sediment bioturbation throughout. The overlying Danian
348 mudstone (Interval 5) contains ostracods ([Fig. 3D](#)) and rare Paleocene planktonic ([Fig. 5](#)) and benthic
349 foraminifera (see text). Small rectangles mark position of photomicrographs shown in [Fig. 3](#). (C) polished
350 slab of Interval 4. (D) Photomicrograph showing oblique section of 2-mm wide burrow filled with finer-
351 grained skeletal-microbioclastic wackestone containing Maastrichtian benthic foraminifer *Fleuryana*
352 *adriatica*. Inset shows a magnification of one of calcispheres sparsely distributed throughout Interval 4 (see
353 also [Fig. 3C](#)).

354

355 **Fig. 3** Thin-section photomicrographs (positions marked by small rectangles in Fig. 2B) of the K–Pg
 356 boundary shallow-marine limestones at Likva. (A) Skeletal-peloidal wackestone from the topmost part of
 357 Interval 3 containing abundant benthic foraminifera, ostracods, and Charophyta skeletal remains, as well as
 358 rare Maastrichtian planktonic foraminifera and pithonellid calcispheres. Inset shows a magnified planktonic
 359 foraminifera *Rugoglobigerina* sp. from the central part (dashed frame) . (B) A bioclastic lag at the
 360 lowermost part of the event bed (Interval 4) composed of requieniid rudists. (C) Skeletal-peloidal packstone-
 361 grainstone from the central part of the K–Pg event bed. Inset shows unusual calcispheres from the central
 362 part (dashed frame). (D) Clayey mudstone (K–Pg “clay”) with ostracods that contains tiny planktonic
 363 foraminifera shown on Fig. 5.

364

365 **Fig. 4** SEM images (A-D) of shocked quartz grains showing closely spaced (<2 microns) planar
 366 deformation features (PDFs) and EDS spectra showing their composition. Grains shown in (B) and (C)
 367 display multiple sets of PDFs. Insoluble residuum of the K–Pg event bed (Interval 4).

368

369 **Fig. 5** SEM images of the basal Paleocene (P0-P α zones) planktonic foraminifera isolated from the K–Pg
 370 boundary “clay” of the Likva section (see Fig. 2). (A-B) *Guembelitra cretacea* CUSHMAN. (C)
 371 *Parvularugoglobigerina* cf. *longiapertura* BLOW. (D) *Eoglobigerina eobulloides* (MOROZOVA). (E)
 372 *Woodringina claytonensis* LOEBLICH and TAPPAN. (F) *Parvularugoglobigerina* cf. *extensa* (BLOW). (G-
 373 I) *Praemurica taurica* (MOROZOVA). (J-K) *Globoconusa daubjergensis* (BRÖNNIMANN). (L)
 374 *Chiloguembelina* cf. *morsei* (KLINE). Scale bars 20 μ m.

375

376

377 Supporting information

378

379 **Fig. S1** Overview geological map showing locations of the K–Pg boundary sections at Likva (Brač island,
 380 [this paper](#)) and Majerovica (Hvar island, [Korbar et al., 2015](#)). Green – Cretaceous to Paleocene platform
 381 carbonates. Orange – Eocene carbonates and clastics. Dotted black lines – regional unconformity. Red comb

382 line – major thrust fault. Small black comb symbol - bed strike and dip.

383

384 **Fig. S2 (A-C)** The outcrop photographs of the Cretaceous–Paleogene (K–Pg) succession on western coast
385 of the Likva cove (the island of Brač, Adriatic Sea, Dalmatia, Croatia).

386

387 **Fig. S3** The upper bedding surface of the K–Pg boundary event bed (Interval 4) showing distinct reddish-
388 brown soft-sediment bioturbation. Coastal outcrop 200 m west of Likva cove (the island of Brač, Adriatic
389 Sea, Dalmatia, Croatia). Coin diameter is 24 mm.

390

391 **Table S1.** Platinum-group elements (PGE) and gold (Au) concentrations in limestone samples from the K–
392 Pg boundary Likva section ([Fig. 2A](#)) and chondrite normalization chart.

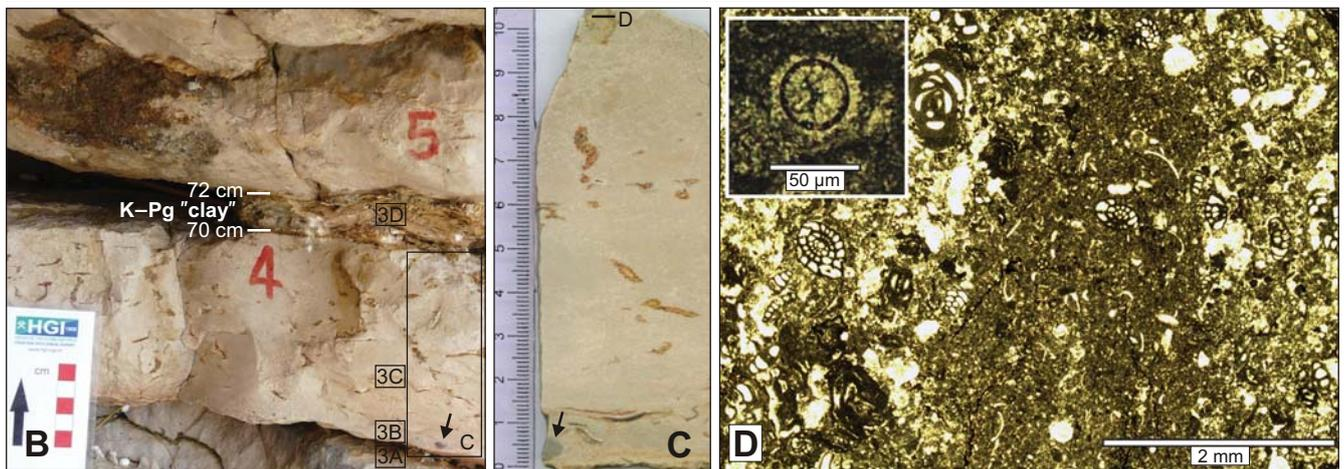
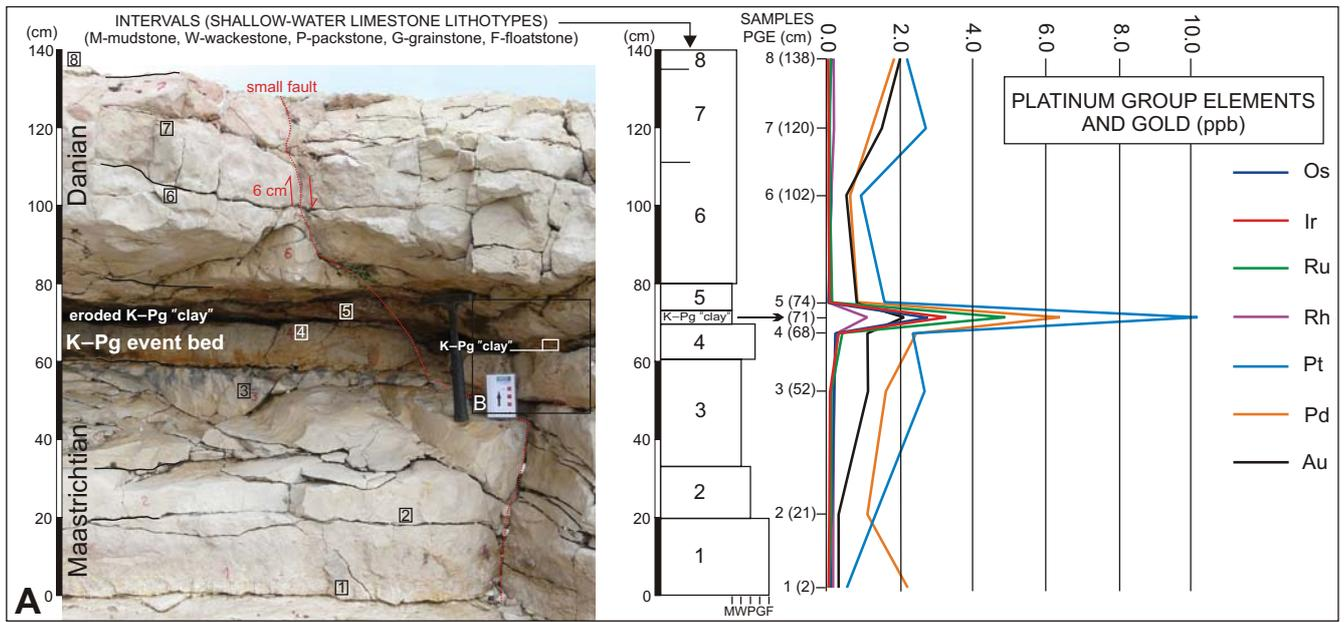
393

394



For Review Only

Page 16 of 45



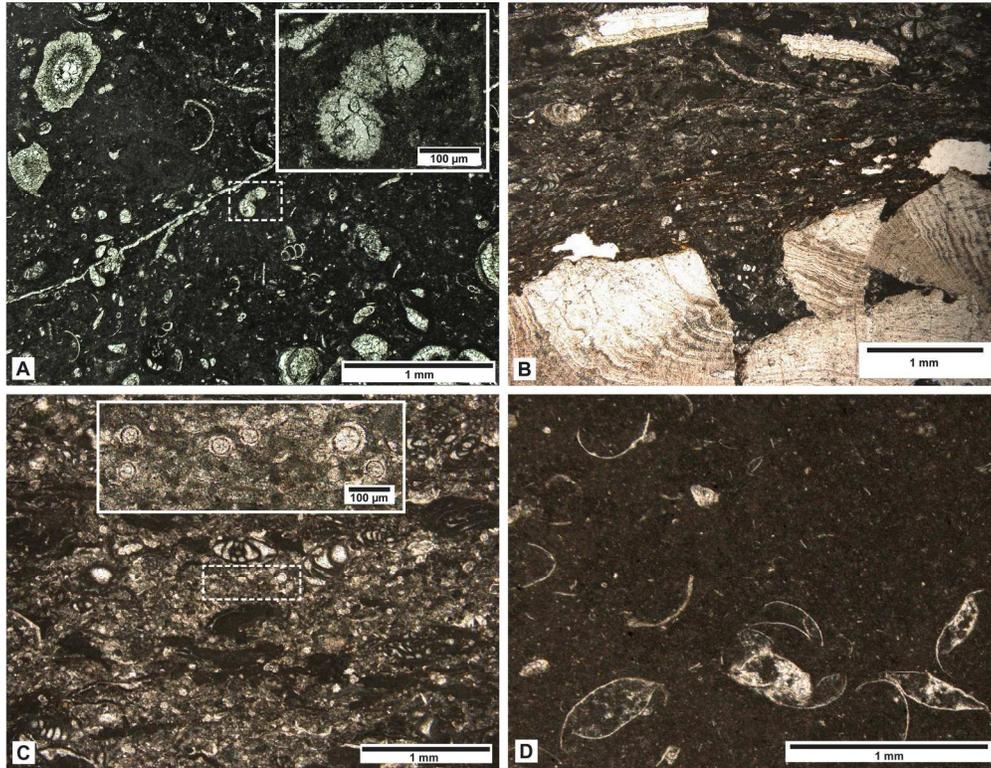


Fig. 3

180x138mm (300 x 300 DPI)

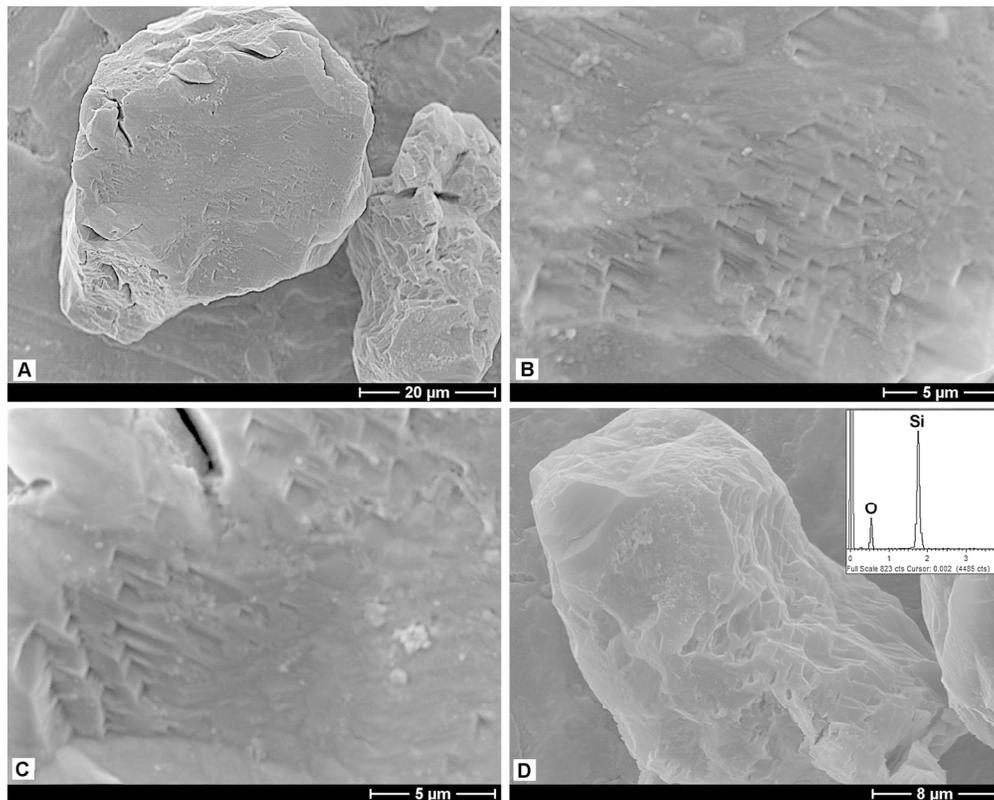


Fig. 4

144x115mm (300 x 300 DPI)

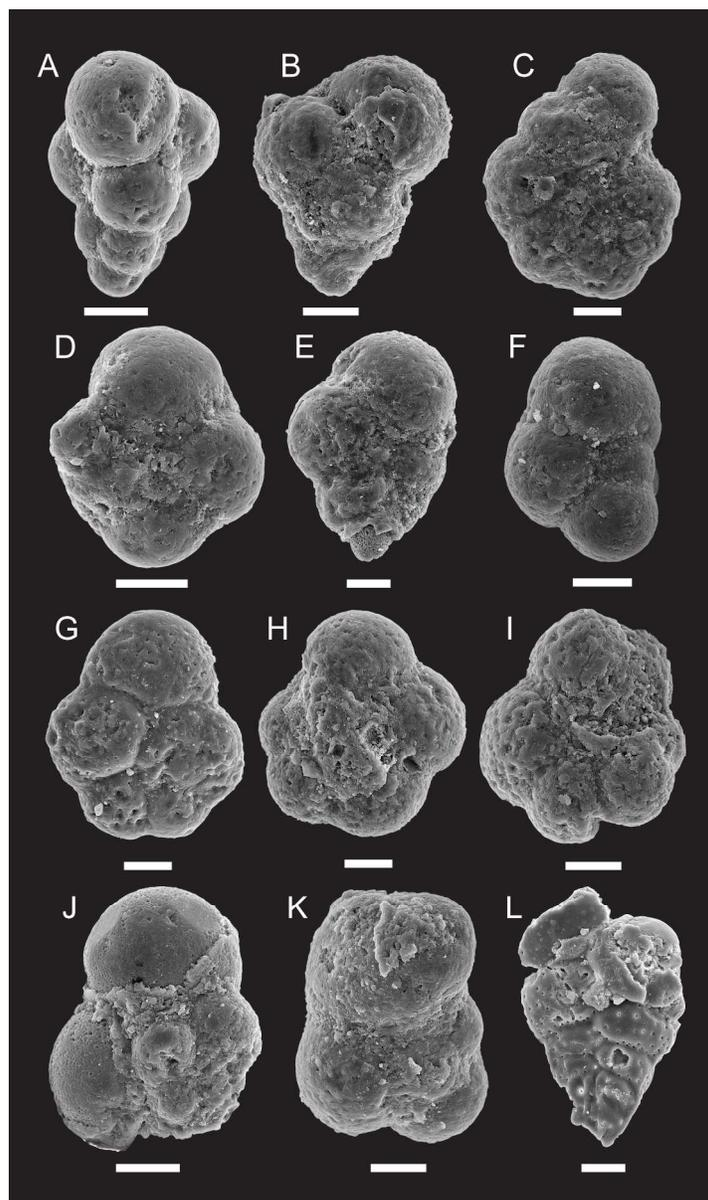
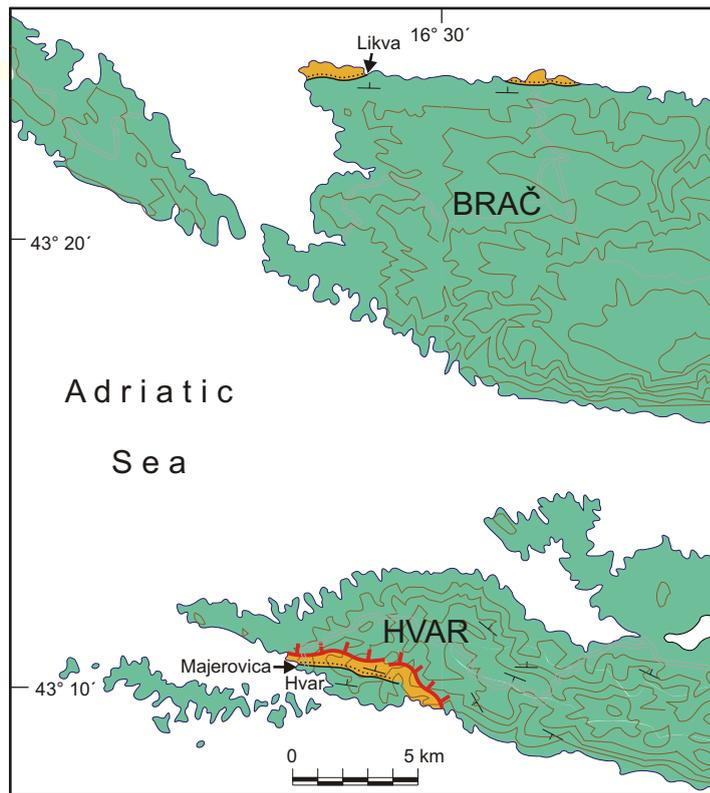


Fig. 5

156x263mm (300 x 300 DPI)

What follows is supplementary material,
which will be made available online but
will not appear in the print version.











1151x649mm (72 x 72 DPI)

Blank corrected concentrations (ppb)

	Os	Ir	Ru	Rh	Pt	Pd	Au	
Int-1		0,02	0,03	0,10	0,10	0,58	2,24	0,35
Int-2		0,09	0,07	0,09	0,14	1,35	1,11	0,30
Int-3		0,04	0,03	0,10	0,11	2,71	1,70	1,16
Int-4		0,39	0,34	0,46	0,18	2,52	2,58	1,04
K-Pg clay		2,86	3,27	4,80	1,03	10,06	6,37	2,12
Int-5		0,09	0,08	0,15	0,08	1,59	0,83	0,80
Int-6		0,10	0,08	0,17	0,07	0,95	0,67	0,56
Int-7		0,17	0,12	0,16	0,16	2,66	1,27	1,48
Int-8		0,06	0,08	0,14	0,20	2,27	1,87	2,02

Blanks

	Os	Ir	Ru	Rh	Pt	Pd	Au	
Blank-A		<0.02	<0.01	0,07	<0.02	0,27	0,24	0,13
Blank-B		<0.02	<0.01	<0.05	0,05	0,32	0,30	0,21

Certified reference materials

	Os	Ir	Ru	Rh	Pt	Pd	Au	
TDB1		0,07	0,12	0,26	0,65	5,48	23,6	6,71
WPR1		11,4	14,3	21,8	12,8	274	228	41,1
WMG1		22,3	48,0	30,0	25,9	748	382	116

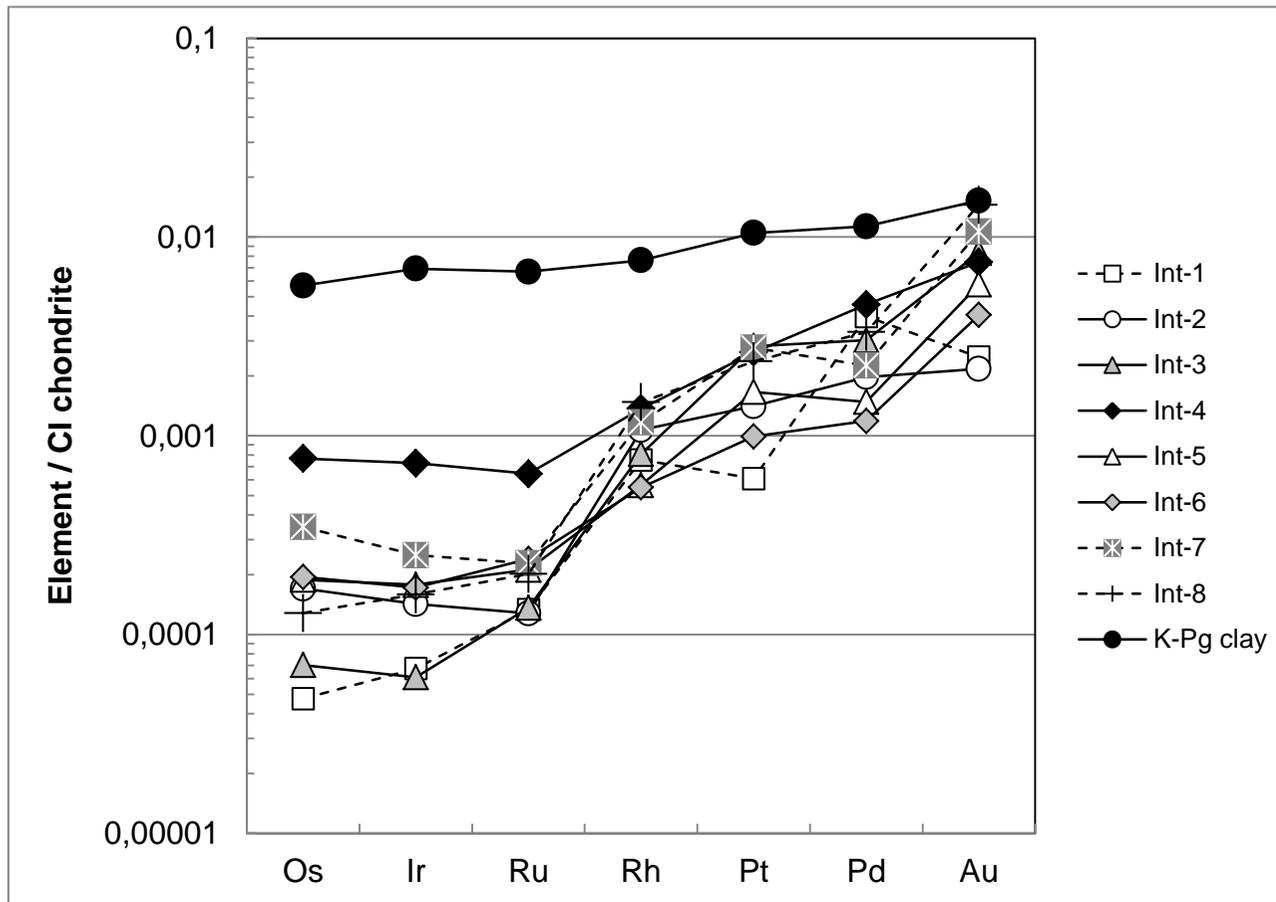
Certified reference materials (Expected values)

	Os	Ir	Ru	Rh	Pt	Pd	Au	
TDB1		0,1	0,15	0,3	0,7	5.8 +/- 1.1	22.4 +/- 1.4	6.3 +/- 1.0
WPR1		11,5	13,5	22	13,4	285	235	43
WMG1		24,1	46,4	34,7	26,3	731	382	110

Samples were prepared by nickel sulfide fire assay with Te co-precipitation. PGE and Au were determined by ICP-MS. Full methodology is given in:

Huber et al. (2001) Geochemistry and petrology of Witwatersrand and Dwyka diamictites from South Africa: search for an extraterrestrial component: *Geochimica et Cosmochimica Acta*, v. 65, p. 2007-2016.

McDonald and Viljoen (2006) Platinum-group element geochemistry of mantle eclogites: a reconnaissance study of xenoliths from the Orapa kimberlite, Botswana. *Appl. Earth Science (Trans. Inst. Min. Metall. B)*, 115, B81-93.



CI chondrite normalized
(Tagle and Berlin 2008)

	502	472	717	135	959	563	139
	Os	Ir	Ru	Rh	Pt	Pd	Au
Int-1	4,76E-05	6,75E-05	1,33E-04	7,55E-04	6,08E-04	3,99E-03	2,49E-03
Int-2	1,70E-04	1,42E-04	1,28E-04	1,07E-03	1,41E-03	1,97E-03	2,17E-03
Int-3	7,02E-05	6,10E-05	1,36E-04	8,10E-04	2,82E-03	3,02E-03	8,34E-03
Int-4	7,69E-04	7,29E-04	6,44E-04	1,37E-03	2,63E-03	4,57E-03	7,48E-03
K-Pg clay	5,70E-03	6,93E-03	6,69E-03	7,63E-03	1,05E-02	1,13E-02	1,53E-02
Int-5	1,89E-04	1,78E-04	2,12E-04	5,65E-04	1,66E-03	1,48E-03	5,78E-03
Int-6	1,95E-04	1,72E-04	2,40E-04	5,50E-04	9,93E-04	1,19E-03	4,05E-03
Int-7	3,47E-04	2,51E-04	2,28E-04	1,17E-03	2,77E-03	2,26E-03	1,07E-02
Int-8	1,28E-04	1,59E-04	2,01E-04	1,48E-03	2,37E-03	3,33E-03	1,45E-02

Chondrite normalised PGE ratios

	[Os/Ir]N	[Ru/Ir]N	[Rh/Ir]N	[Pt/Ir]N	[Pd/Ir]N	[Ru/Rh]N
Int-1	0,71	1,97	11,19	9,02	59,10	0,18
Int-2	1,20	0,90	7,51	9,90	13,87	0,12
Int-3	1,15	2,24	13,29	46,32	49,59	0,17
Int-4	1,05	0,88	1,88	3,60	6,28	0,47
K-Pg clay	0,82	0,97	1,10	1,51	1,63	0,88
Int-5	1,06	1,19	3,18	9,34	8,33	0,38
Int-6	1,13	1,39	3,19	5,76	6,89	0,44
Int-7	1,39	0,91	4,66	11,06	9,00	0,19
Int-8	0,81	1,27	9,27	14,88	20,89	0,14

0,63 0,754317

0,75 0,898589

0,78 0,934902

0,29 0,344347

0,74 0,890167

0,83 0,997595

0,88 1,052635

0,62 0,743591

0,57 0,689753

